Decay vertex reconstruction and 3-dimensional lifetime determination at BESIII*

XU Min(徐敏)[1,2;1)] HE Kang-Lin(何康林)[2;2)] ZHANG Zi-Ping(张子平)[1] WANG Yi-Fang(王贻芳)[2]
BIAN Jian-Ming(边渐鸣)[2,3] CAO Guo-Fu(曹国富)[2,3] CAO Xue-Xiang(曹学香)[2,3]
CHEN Shen-Jian(陈申见)[4] DENG Zi-Yan(邓子艳)[2] FU Cheng-Dong(傅成栋)[2]
GAO Yuan-Ning(高原宁)[5] HAN Lei(韩磊)[6] HAN Shao-Qing(韩少卿)[7] HE Miao(何苗)[2]
HU Ji-Feng(胡继峰)[3] HU Xiao-Wei(胡小为)[4] HUANG Bin(黄彬)[2,3] HUANG Xing-Tao(黄性涛)[8]
JIA Lu-Kui(贾卢魁)[2,3] JI Xiao-Bin(季晓斌)[2] LI Hai-Bo(李海波)[2] LI Wei-Dong(李卫东)[2]
LIANG Yu-Tie(梁羽铁)[9] LIU Chun-Xiu(刘春秀)[2] LIU Huai-Min(刘怀民)[2] LIU Ying(刘颖)[10]
LIU Yong(刘勇)[2,3] LUO Tao(罗涛)[2,3] LÜ Qi-Wen(吕绮雯)[11] MA Qiu-Mei(马秋梅)[2]
MA Xiang(马想)[2,3] MAO Ya-Jun(冒亚军)[9] MAO Ze-Pu(毛泽普)[2] MO Xiao-Hu(莫晓虎)[2]
NING Fei-Peng(宁飞鹏)[11] PING Rong-Gang(平荣刚)[2] QIU Jin-Fa(邱进发)[2] SONG Wen-Bo(宋文博)[12]
SUN Sheng-Sen(孙胜森)[2] SUN Xiao-Dong(孙晓东)[2,3] SUN Yong-Zhao(孙永昭)[2]
TIAN Hao-Lai(田浩来)[2,3] WANG Ji-Ke(王纪科)[2,3] WANG Liang-Liang(王亮亮)[2,3]
WEN Shuo-Pin(文硕频)[2] WU Ling-Hui(伍灵慧)[2,3] WU Zhi(吴智)[2,3] XIE Yu-Guang(谢宇广)[2]
YAN Jie(言杰)[1] YAN Liang(严亮)[2,3] YAO Jian(姚剑)[12] YUAN Chang-Zheng(苑长征)[2]
YUAN Ye(袁野)[2] ZHANG Chang-Chun(张长春)[2] ZHANG Jian-Yong(张建勇)[2]
ZHANG Lei(张雷)[4] ZHANG Xue-Yao(张学尧)[8] ZHANG Yao(张瑶)[2] ZHENG Yang-Heng(郑阳恒)[3]
ZHU Yong-Sheng(朱永生)[2] ZOU Jia-Heng(邹佳恒)[8]

1 (Department of Modern Physics, University of Science and Technology of China, Hefei 230026, China)
2 (Institute of High Energy Physics, CAS, Beijing 100049, China)
3 (Graduate University of Chinese Academy of Sciences, Beijing 100049, China)
4 (Nanjing University, Nanjing 210093, China)
5 (Tsinghua University, Beijing 100084, China)
6 (Henan Normal University，Henan 453007，China)
7 (Nanjing Normal University, Nanjing 210097, China)
8 (Shandong University, Jinan 250100, China)
9 (Peking University, Beijing 100871, China)
10 (Guangxi University, Nanning 530004, China)
11 (Shanxi University, Taiyuan 003006, China)
12 (Zhengzhou University, Zhengzhou 450001, China)

Abstract This paper focuses mainly on the vertex reconstruction of resonance particles with a relatively long lifetime such as K^0_S, Λ, as well as on lifetime measurements using a 3-dimensional fit. The kinematic constraints between the production and decay vertices and the decay vertex fitting algorithm based on the least squares method are both presented. Reconstruction efficiencies including experimental resolutions are discussed. The results and systematic errors are calculated based on a Monte Carlo simulation.

Key words decay vertex, resolution of decay length, lifetime, reconstruction efficiency

PACS 13.25.Es, 13.30.Eg, 07.05.Kf

Received 9 September 2008, Revised 25 November 2008

* Supported by CAS Knowledge Innovation Project (112901160333, 111087513811), National Natural Science Foundation of China (10491300, 10491303) and 100 Talents Program of CAS (U-25 and U-54)

1) E-mail: xum@ihep.ac.cn

2) E-mail: hekl@ihep.ac.cn

1 Introduction

The reconstruction of vertices plays an important role in high energy physics analysis. In the time of bubble chamber experiments, vertex fits were one of the primary means of particle identification. Secondary vertices and their associated tracks could be recognized visually. In today's collider experiment, the primary vertex is inside the beam tube, whereas tracks are reconstructed outside and extrapolated back in order to reconstruct the primary and secondary decay vertices.

The Beijing Spectrometer (BES) III[1, 2] is an upgraded detector at the Beijing Electron Positron Collider (BEPC) II for probing τ-charm physics. It consists of a beryllium beam pipe, a helium-based small-celled drift chamber, a Time-Of-Flight (TOF) device, a CsI(Tl) crystal calorimeter, a super-conducting solenoidal magnet with a field of 1 tesla, and a muon identifier of Resistive Plate Counters (RPC) interleaved with the magnet yoke plates. A preliminary version of the BES Offline Software System (BOSS)[3] has been implemented successfully. The detector simulation[4] is based on Geant4[5].

Resonance particles with relatively long lifetimes, such as K^0_S and $\Lambda/\bar{\Lambda}$, etc., are abundantly produced in the τ-charm energy region. At BESIII, a series of algorithms is developed to identify these particles in both reconstruction and analysis environments. The reconstruction of vertices serves the purpose of improving the precision of momentum vectors of tracks emerging from a common space point. The kinematic constraints between the vertices of particle production and decay are applicable to suppress the background in physics analysis.

2 Kinematic constraints between the production and decay vertices

To introduce this subject the schematic diagram in Fig. 1 is taken as an example: it shows a resonance particle K^0_S decaying to $\pi^+\pi^-$ at a secondary vertex after being produced in the beam interaction region. The distance between its primary production point near the beam center and decay point to $\pi^+\pi^-$ daughters is called the "flight distance" s, which is related to its proper time $c\tau$ in units of distance through the relativistic formula (c is the velocity of light)

$$s=\beta ct=\gamma\beta c\tau=\frac{p}{m}c\tau\,, \tag{1}$$

where p and m are the momentum and mass of the resonance particle. Denoting the coordinates of the production point as $(x_\mathrm{p},y_\mathrm{p},z_\mathrm{p})$ and the decay point as $(x_\mathrm{d},y_\mathrm{d},z_\mathrm{d})$, in a fixed solenoidal magnetic field the solutions of the equations of motion for a neutral particle are straight lines,

$$\begin{aligned} x_\mathrm{p}-x_\mathrm{d}+\frac{p_x}{m}c\tau=0,\\ y_\mathrm{p}-y_\mathrm{d}+\frac{p_y}{m}c\tau=0,\\ z_\mathrm{p}-z_\mathrm{d}+\frac{p_z}{m}c\tau=0, \end{aligned} \tag{2}$$

and helixes for a charged particle

$$\begin{aligned} x_\mathrm{p}-x_\mathrm{d}+\frac{p_x}{a}\sin(ac\tau/m)+\frac{p_y}{a}(1-\cos(ac\tau/m))=0,\\ y_\mathrm{p}-y_\mathrm{d}+\frac{p_y}{a}\sin(ac\tau/m)-\frac{p_x}{a}(1-\cos(ac\tau/m))=0,\\ z_\mathrm{p}-z_\mathrm{d}+\frac{p_z}{m}c\tau=0, \end{aligned} \tag{3}$$

where $a=-cBQ$, B is the field strength in Tesla, and Q is the charge, (p_x,p_y,p_z) is the 3-momentum at the decay point.

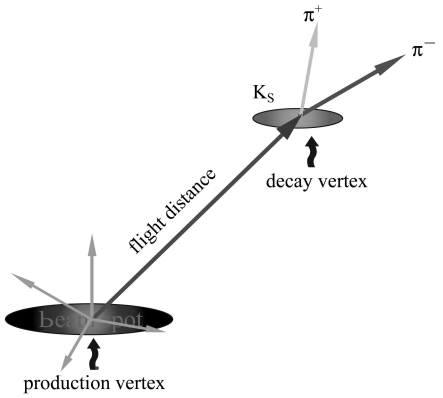

Fig. 1. Scheme of the kinematics between the production and decay vertices of K^0_S.

The three equations (Eq. (2) or Eq. (3)) provide three constraints, so for one unknown $c\tau$ a total of two degrees of freedom remains. To solve for $c\tau$ and its error, the variables in the constraint equations are classified into two categories: known ($\boldsymbol{\alpha}$) with errors and unknown ($c\tau$). The vector $\boldsymbol{\alpha}$ contains 10 variables, which are the 4-momentum plus the coordinates of the production and decay points, i.e.

$$\boldsymbol{\alpha}=(p_x,p_y,p_z,E,x_\mathrm{d},y_\mathrm{d},z_\mathrm{d},x_\mathrm{p},y_\mathrm{p},z_\mathrm{p})^\mathrm{T}\,.$$

The constraint equations can be written generally as $\boldsymbol{H}(\boldsymbol{\alpha},c\tau)=0$. Expanding around a convenient point $(\boldsymbol{\alpha}_\mathrm{A},c\tau_\mathrm{A})$ yields the linearized constraint equations

$$\boldsymbol{D}\delta\boldsymbol{\alpha}+\boldsymbol{E}\delta c\tau+\boldsymbol{d}=0\,,$$

where $\boldsymbol{D}$ and $\boldsymbol{E}$ are the derivatives of $\boldsymbol{H}$ with respect to $\boldsymbol{\alpha}$ and $c\tau$, respectively, $\delta\boldsymbol{\alpha}=\boldsymbol{\alpha}-\boldsymbol{\alpha}_\mathrm{A}$, $\delta c\tau=c\tau-c\tau_\mathrm{A}$, and $\boldsymbol{d}=\boldsymbol{H}(\boldsymbol{\alpha}_\mathrm{A},c\tau_\mathrm{A})$, and $c\tau$ can be solved through an iteration process. Initially, $\boldsymbol{\alpha}_\mathrm{A}$ can be set to the

values of track parameters calculated from the decay vertex finding algorithm and predetermined production point, and $c\tau_{\rm A}$ can be set to zero. The constraints are incorporated using the method of Lagrange multipliers in which the χ^2 is written as a sum of two terms, e.g.

$$\chi^2=(\boldsymbol{\alpha}-\boldsymbol{\alpha}_0)^{\rm T}\boldsymbol{V}_{\boldsymbol{\alpha}0}^{-1}(\boldsymbol{\alpha}-\boldsymbol{\alpha}_0)+2\boldsymbol{\lambda}^{\rm T}(\boldsymbol{D}\delta\boldsymbol{\alpha}+\boldsymbol{E}\delta c\tau+\boldsymbol{d}),$$

where $\boldsymbol{\alpha}_0$ and $\boldsymbol{V}_{\boldsymbol{\alpha}0}$ are the initial track parameters and their covariance matrix, $\boldsymbol{\lambda}$ is a vector of the Lagrange multinomial.

The solution of $c\tau$ and its covariance matrix can be obtained by minimizing the χ^2 with respect to $\boldsymbol{\alpha}$, $c\tau$ and $\boldsymbol{\lambda}$. After some matrix algebra, one gets

$$\delta c\tau=-\boldsymbol{V}_{c\tau}\boldsymbol{E}^{\rm T}\boldsymbol{\lambda}_0,\quad \boldsymbol{V}_{c\tau}=(\boldsymbol{E}^{\rm T}\boldsymbol{V}_{\rm D}\boldsymbol{E})^{-1}.$$

The auxiliary quantities $\boldsymbol{\lambda}_0$ and $\boldsymbol{V}_{\rm D}$ are defined as

$$\boldsymbol{\lambda}_0=\boldsymbol{V}_{\rm D}(\boldsymbol{D}\delta\boldsymbol{\alpha}_0+\boldsymbol{d}),\quad \boldsymbol{V}_{\rm D}=(\boldsymbol{D}\boldsymbol{V}_{\boldsymbol{\alpha}0}\boldsymbol{D}^{\rm T})^{-1},$$

where $\delta\boldsymbol{\alpha}_0=\boldsymbol{\alpha}_0-\boldsymbol{\alpha}_{\rm A}$. The same mechanism also yields the updated $\boldsymbol{\alpha}$ measurements

$$\boldsymbol{\alpha}=\boldsymbol{\alpha}_0-\boldsymbol{V}_{\boldsymbol{\alpha}0}\boldsymbol{D}^{\rm T}\boldsymbol{\lambda},\quad \boldsymbol{\lambda}=\boldsymbol{\lambda}_0+\boldsymbol{V}_{\rm D}\boldsymbol{E}\delta c\tau,$$

as well as their covariance matrix and the correlation with $c\tau$:

$$\begin{aligned}\boldsymbol{V}_{\boldsymbol{\alpha}} &= \boldsymbol{V}_{\boldsymbol{\alpha}0}-\boldsymbol{V}_{\boldsymbol{\alpha}0}\boldsymbol{D}^{\rm T}\boldsymbol{V}_{\rm D}\boldsymbol{D}\boldsymbol{V}_{\boldsymbol{\alpha}0}+\\ &\quad \mathrm{cov}(\boldsymbol{\alpha},c\tau)\boldsymbol{V}_{c\tau}^{-1}\mathrm{cov}^{\rm T}(\boldsymbol{\alpha},c\tau),\\ \mathrm{cov}(\boldsymbol{\alpha},c\tau) &= -\boldsymbol{V}_{\boldsymbol{\alpha}0}\boldsymbol{D}^{\rm T}\boldsymbol{V}_{\rm D}\boldsymbol{E}\boldsymbol{V}_{c\tau}.\end{aligned}$$

χ^2 is given by

$$\chi^2=\boldsymbol{\lambda}^{\rm T}(\boldsymbol{D}\delta\boldsymbol{\alpha}_0+\boldsymbol{d}).$$

From the solution of $c\tau$ and its error($\boldsymbol{V}_{c\tau}$), one can see that precision measurement of the lifetime requires both the beginning and endpoint of the particle flight vector to be determined accurately. The beginning point is well determined by the beam spot size perhaps by other tracks in the production region[6]. The endpoint is determined by fitting decay vertices which will be described in the next section, and its measurement accuracy is determined purely by the tracking errors of the daughter particles.

3 Geometrical fit of $\mathrm{K_S^0}$ and $\Lambda/\bar{\Lambda}$ decay vertices

In the BESIII experiment, "V" type secondary vertices are mostly encountered in the physics analysis and event reconstruction, such as the decay vertices of $\mathrm{K_S^0}$ and $\Lambda/\bar{\Lambda}$, the interaction vertices of γ-conversion, etc. These vertices are formed by two charged tracks. To find the secondary vertices, daughter tracks are forced to pass the common point in space which can be determined by constraint equations[7].

In a solenoidal B field, for a set of n tracks (parameterized by $\boldsymbol{\alpha}_i=(p_x,p_y,p_z,E,x,y,z)_i^{\rm T}$, $i=(1,\cdots,n)$) forced to pass through a common point $\boldsymbol{x}=(x,y,z)$, each charged track i has two constraints, corresponding to the bent and non-bent planes, respectively. The constraint equations relating to the track parameter and vertex position have the following forms:

$$\begin{aligned}&p_{xi}\Delta y_i-p_{yi}\Delta x_i-\frac{a_i}{2}(\Delta x_i^2+\Delta y_i^2)=0,\\ &\Delta z_i-\frac{p_{zi}}{a_i}\sin^{-1}[a_i(p_{xi}\Delta x_i+p_{yi}\Delta y_i)/p_{Ti}^2]=0,\end{aligned}\tag{4}$$

where $\Delta x_i=x_x-x_i$, x_x is the vertex position, x_i is the point at track i. $a_i=-cBQ_i$, Q_i is the charge, B is the magnetic field and p_{Ti} is the transverse momentum.

The coordinates of the decay vertices can be obtained by applying a least squares method:

$$\begin{aligned}\chi^2 &= (\boldsymbol{\alpha}-\boldsymbol{\alpha}_0)^{\rm T}\boldsymbol{V}_{\boldsymbol{\alpha}_0}^{-1}(\boldsymbol{\alpha}-\boldsymbol{\alpha}_0)+\\ &\quad (\boldsymbol{x}-\boldsymbol{x}_0)^{\rm T}\boldsymbol{V}_{\boldsymbol{x}_0}^{-1}(\boldsymbol{x}-\boldsymbol{x}_0)+\\ &\quad 2\boldsymbol{\lambda}^{\rm T}(\boldsymbol{D}\delta\boldsymbol{\alpha}+\boldsymbol{E}\delta\boldsymbol{x}+\boldsymbol{d}),\end{aligned}\tag{5}$$

where $\boldsymbol{\alpha}=(\boldsymbol{\alpha}_0,\boldsymbol{\alpha}_1,\cdots,\boldsymbol{\alpha}_n)^{\rm T}$ are the track parameters of the daughter tracks, $\boldsymbol{x}=(x,y,z)$ is the coordinate vector of the decay vertex, $V_{\boldsymbol{\alpha}}$ and $V_{\boldsymbol{x}}$ are their covariance matrices. $\delta\boldsymbol{\alpha}=\boldsymbol{\alpha}-\boldsymbol{\alpha}_{\rm A}$, $\delta\boldsymbol{x}=\boldsymbol{x}-\boldsymbol{x}_{\rm A}$ and $\boldsymbol{\lambda}$ is a vector with Lagrange multipliers as components. The subscript "0" denotes the initial values, while "A" denotes the expansion point. The matrices of $\boldsymbol{D}$ and $\boldsymbol{E}$ are the derivatives of the constraints with respect to the track parameters and the vertex point. The matrix $\boldsymbol{d}$ is a constant term built up from the constraints.

The solution of Eq. (5) is similar to the procedure for solving $c\tau$ described in Section 2. The mother particle, including the track parameters and covariance matrix, is constructed by shifting its daughter's track parameters and covariance matrices to the vertex position. The correlations between tracks introduced by the vertex constraint must be taken into account when recalculating the daughter parameters and their covariance matrices.

4 $\mathrm{K_S^0}$ reconstruction and selection

Neutral kaons are produced plentifully in $\mathrm{J/\psi}$ and charmed meson decays. For a large decay branching ratio and clean background contamination, events of $\mathrm{J/\psi\to K^{*0}\bar{K}^0}$ with $\mathrm{K^{*0}\to K^{\pm}\pi^{\mp}}$ and $\mathrm{\bar{K}^0\to K_S^0\to}$

$\pi^+\pi^-$ are generated for the study of K^0_S reconstruction.

The event selection proceeds as follows. All charged tracks are required to be well measured by MDC with $|\cos\theta| < 0.93$, where θ is the polar angle. For K^0_S decay daughters, the track parameters are required to satisfy $|d_z| < 40$ cm, where d_z is the coordinate of the point of closest approach to the origin along the z direction. Tracks that are not associated with a K^0_S decay are required to stem from the interaction point, with $|d_\rho| <1$ cm and $|d_z| < 5$ cm, where d_ρ is the closest distance (including its sign) to the origin in the xy plane. A track is classified as a charged pion or a charged kaon by using the likelihood which combines the TOF and dE/dx information. The track parameters and their covariance matrices are corrected for energy losses and multiple scattering according to the assigned particle hypotheses in the Kalman track fitting procedure. Appropriate combinations of $\pi^+\pi^-$ and $K^\pm\pi^\mp$ pairs are selected for K^0_S reconstruction and the performance studies. The invariant mass distributions of all $\pi^+\pi^-$ pairs are shown in Fig. 2(a).

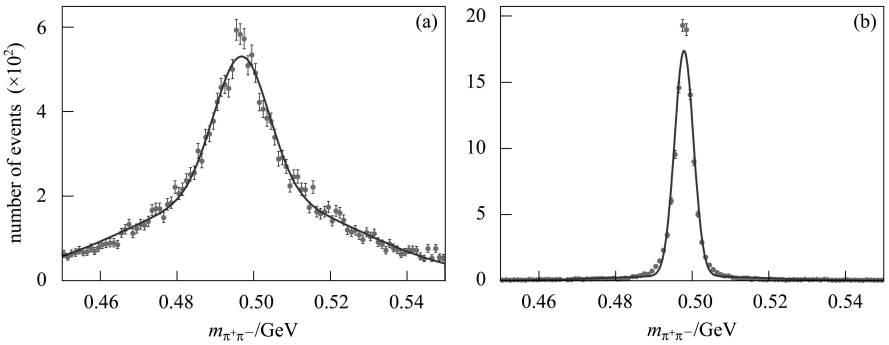

Fig. 2. Invariant mass distribution of $\pi^+\pi^-$ pairs before (a) and after (b) secondary vertex reconstruction. The signal part is fitted with a Gaussian function while the background part is represented by a 2nd-order Chebychev polynomial function.

Each $\pi^+\pi^-$ combination is subjected to the secondary vertex reconstruction program. The resulting mass distribution is shown in Fig. 2(b). After secondary vertex reconstruction, the K^0_S mass resolutions are significantly improved since the vector momentum of each track is recalculated at the mutual crossing point rather than at the point of closest approach to the origin. Similar results could be obtained in Λ baryon reconstructions.

The secondary vertices are somewhat apart from the interaction point, so cutting on the decay length (L) is useful to suppress backgrounds effectively, where L is the displacement from the primary vertex to the decay vertex. To optimize the K^0_S selection criteria, simulated $\psi'' \to D\bar{D}$ data are investigated.

In the $\psi'' \to D\bar{D}$ Monte Carlo data sample, all pairs of oppositely charged tracks are considered. Fig. 3(a) shows the mass distribution of the candidate which is calculated at the vertex. In the mass range of 0.48—0.52 GeV/c^2, a clear peak appears around the mass of the K^0_S, and the combinatorial backgrounds distribute approximately uniformly. To extract the ratio of the decay length to its error (L/σ_L) for the signals and backgrounds, three mass windows are opened in Fig. 3(a): one signal region is within a $\pm 3\sigma$ window centered at the nominal K^0_S mass; two sideband regions are in the window of $(-6.5,-3.5)\sigma$ and $(3.5,6.5)\sigma$ deviated from the nominal K^0_S mass, where $\sigma(\sim 2$ MeV) is the mass resolution of K^0_S. The corresponding L/σ_L's in the sideband regions are drawn in Fig. 3(b), which represent the combinatorial backgrounds. Fig. 3(c) shows the distribution of L/σ_L after background subtraction, which represents the K^0_S signal. The peak near zero in Fig. 3(b) shows that most of the combinatorial tracks come from the interaction point. Negative decay lengths are obtained for a small fraction of K^0_S signals in Fig. 3(c), which is caused by the limited detector resolution. Fig. 3(d) shows the signal efficiencies and background contamination rate variations with the L/σ_L selection criteria. While increasing the cut value of L/σ_L, the combinatorial backgrounds decline more quickly than the K^0_S signal, especially in the region of $-2 < L/\sigma_L < 2$. The typical value of σ_L is ~ 1 mm in K^0_S reconstruction.

If in the case of Fig. 3(d) we take $L/\sigma_L > 2$, corresponding to $L > 2$ mm, the achieved $R_{S/B}$ values (the ratio of signal to background) are reasonably acceptable for most physics analyses. The detailed event selection criteria rely on the momentum of the K^0_S, the background level, the inconsistency between the data and the Monte Carlo simulation. One may

therefore vary the K^0_S selection criteria in different physics analyses. For example, decay modes of $K^0_S\pi^+$, $K^0_S\pi^+\pi^+\pi^-$ and $K^0_S\pi^+\pi^0$ are often to be reconstructed as D^+ tags. The loose K^0_S cut may be chosen in $K^0_S\pi^+$ mode since the background level is very low in the final state, but more stringent K^0_S selection criteria have to be adopted in $K^0_S\pi^+\pi^+\pi^-$ and $K^0_S\pi^+\pi^0$ modes to cut down the combinatorial background.

By following the procedure described above, a series of curves with various selection criteria in different K^0_S momentum ranges for signal efficiency and background rate can be obtained to optimize $R_{S/B}$ and to reduce systematic uncertainties. The detailed K^0_S selection criteria can be determined by comparing data and Monte Carlo simulation in each momentum bin; one can create a look-up-table to help people to optimize their analysis.

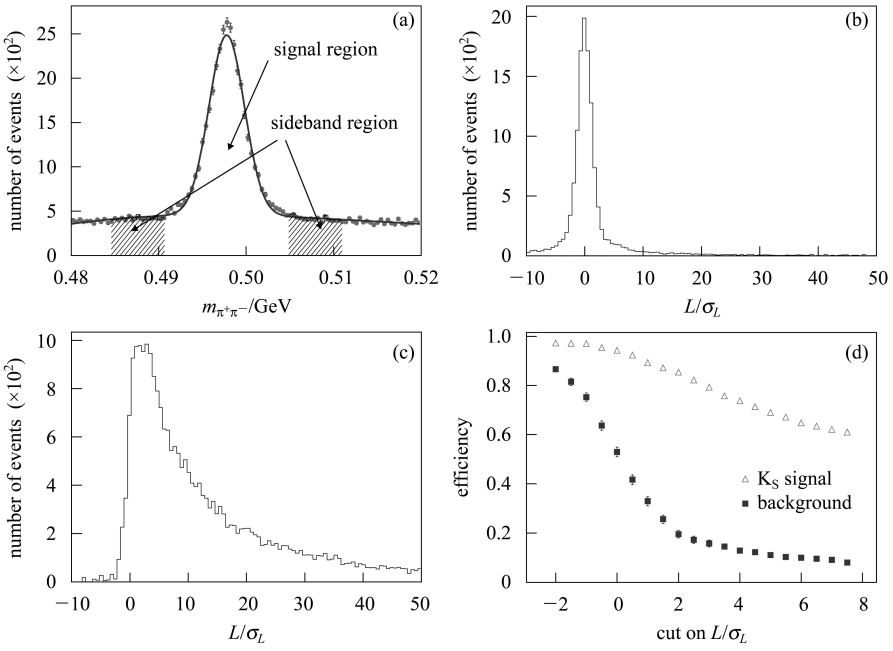

Fig. 3. (a) Mass distribution of reconstructed $\pi^+\pi^-$ pairs in the $\psi'' \to D\bar{D}$ Monte Carlo sample; (b) L/σ_L distribution for the combinatorial backgrounds; (c) L/σ_L distribution for the K^0_S signal; (d) signal efficiencies and background contamination rate variations with L/σ_L. Circles: K^0_S signal, squares: combinatorial background.

5 Lifetime measurement

Like the invariant mass, lifetime is a proper quantity of resonance particles in high energy physics, which is closely interrelated with the particle's decay width. A relatively long living particle travels a certain distance before decaying into its daughters in the detector.

Supposing we want to measure the lifetime of the decay of a particle in a generic particle physics experiment; the first step in this measurement is to collect a data sample with observed decays. Each decay is described by a decay time, which is derived from a flight distance between the production vertex and decay vertex as shown in Fig. 1. For an ideal detector the distribution of observed decay times is an exponential function with an exponent that is the inverse of the lifetime τ:

$$f(t) = \exp(-t/\tau). \tag{6}$$

A real detector has a finite experimental resolution and detection efficiency on each measurement of the decay time t. The measured decay time distribution is a convolution of the ideal decay time (t'), the detection efficiency (ϵ) and experimental resolution (G):

$$h(t) = \int_{-\infty}^{+\infty} \mathrm{d}t' \exp(-t'/\tau)\cdot\epsilon(t')\cdot G(t,t'), \tag{7}$$

where ϵ and G must be determined from the control sample.

The decay of $J/\psi \to K^{*0}K^0_S$ with $K^{*0} \to K^\pm\pi^\mp$ is an "ideal" control sample. The data are generated in two ways: one for a control sample in which the lifetime of K^0_S is set to be twice its nominal value[8]; another for a test sample where the lifetime of K^0_S is set to be its nominal value. The K^0_S's are tagged by the reconstructed $K^* \to K\pi$ in the above two sam-

ples, where the charged pion and kaon are required to come from the interaction point. The distributions of the invariant mass for each $K\pi$ pair and its recoiling mass are shown in Fig. 4(a) and Fig. 4(b). About 24000 tagged K^0_S's are observed in 50000 generated samples. The detection efficiency can thus be determined by counting the reconstructed K^0_S's in the tagged samples.

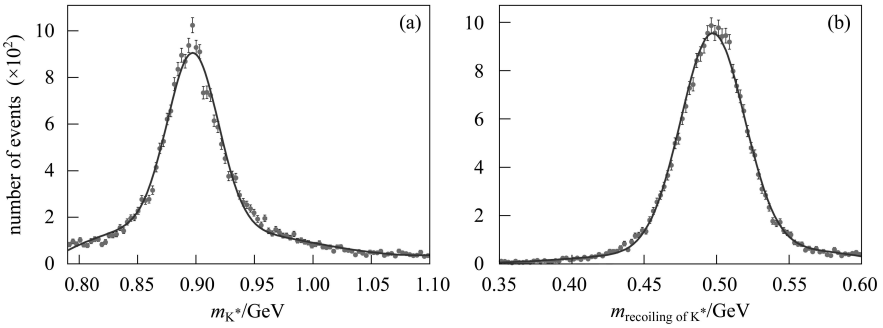

Fig. 4. (a) Invariant mass distribution for $K^{\mp}\pi^{\pm}$ pairs and (b) the corresponding recoiling mass distribution in control samples.

5.1 Experimental resolutions

The error of the decay length depends on the accuracies of the decay vertex and production vertex, which may vary with the value of the decay length. As a first approximation, we assume that the resolution function is invariant over all decay lengths. Thus we can evaluate the resolution function in several ways: the ρ^0 decay in $J/\psi \to \rho^0\pi^0$; the K^{*0} decay in $J/\psi \to K^{*0}K^0_S$; the combinatorial background sample in K^0_S sidebands as shown in Fig. 3. Except for the decay length (always equal to 0 for the above samples), the kinematic features of the two track vertices formed by the $\pi^+\pi^-$ or $K^{\mp}\pi^{\pm}$ pair are similar to that of the K^0_S decay vertex. Fig. 5(a) shows $\bar{\sigma}_L$ for the ρ^0 decay, the K^{*0} decay, the combinatorial background

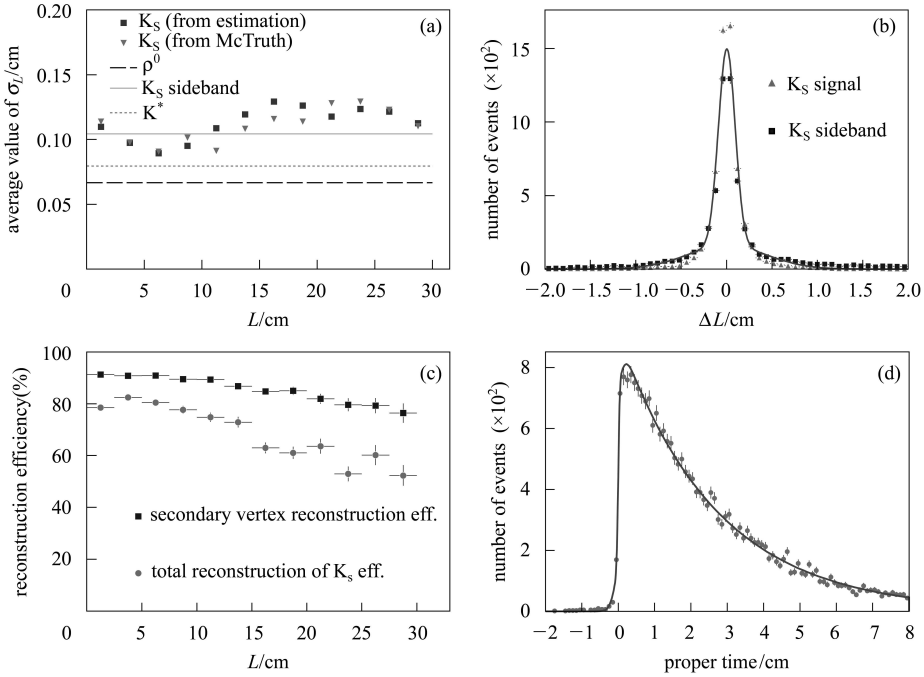

Fig. 5. (a) The square points represent $\bar{\sigma}_L$ for the K^0_S signal from estimation, the triangular points represent the resolution of the decay length by using Monte Carlo truth information, the $\bar{\sigma}_L$ calculated from the ρ^0 decay, the K^{*0} decay and the K^0_S sideband events are shown by the dashed line, the dotted line and the solid line, respectively; (b) the square and triangle points represent the ΔL distribution for the events from the K^0_S signal and sideband regions, the smooth line represents the experimental resolution function after $\bar{\sigma}_L$ correction; (c) the circles and square points represent the efficiencies of the K^0_S reconstruction and secondary vertex reconstruction; and (d) the K^0_S proper time distribution and fit.

and the K^0_S decay for different measured decay lengths, where $\bar{\sigma}_L$ is the average value of σ_L which is calculated by the program of secondary vertex reconstruction. Supposing the detector resolution is proportional to $\bar{\sigma}_L$, we can model the detector resolution with the events from the K^0_S sideband. The sample from the ρ^0 decay and the K^{*0} decay can be used to study the systematic errors.

Figure 5(b) shows the ΔL distributions for the combinatorial backgrounds and the K^0_S signal, where $\Delta L = L_{\rm measure} - L_{\rm truth}$ is the difference between the measured decay length ($L_{\rm measure}$) and the generated decay length ($L_{\rm truth}$). For the combinatorial backgrounds, $L_{\rm truth} = 0$; and for the K^0_S signal, $L_{\rm truth}$ can be read out in the Monte Carlo generation. The ΔL distribution of combinatorial backgrounds can be fitted by a double Gaussian which represents the detector resolution, and a 2nd-order polynomial which represents the background contamination. There are six parameters to model the experimental resolution. They are: f_i representing the fractions, μ_i representing the shift of peak values and σ_i standing for the resolutions, where $i = 1, 2$, $\mu_1 = \mu_2$ is required in the fit. To address the resolution function in different ranges of the decay length, the σ_i's are scaled by a factor of $\bar{\sigma}_L(L)|_{\rm sig}/\bar{\sigma}_L|_{\rm back}$, where $\bar{\sigma}_L|_{\rm back}$ and $\bar{\sigma}_L(L)|_{\rm sig}$ are the average values of σ_L for the combinatorial backgrounds and the K^0_S signals. The scaled resolution function is also drawn in Fig. 5(b) which is quite consistent with the ΔL distribution of the K^0_S signal.

5.2 Detection efficiencies

Supposing the detection efficiency is 100% , the decay time distribution in Eq. (7) would be predicted as:

$$h(t) = \int_{-\infty}^{+\infty} {\rm d}t' \exp(-t'/\tau) \cdot G(t, t'). \qquad (8)$$

Applying the resolution function G (which is determined from Fig. 5(a)) to Eq. (8), we can get the expected decay length distribution. The detection efficiencies can be extracted by comparing the number of observed and expected events in each bin. Fig. 5(c) shows the dependence of the K^0_S reconstruction efficiency on the decay length, which can be modeled by a 2nd-order polynomial. The efficiency of the secondary vertex reconstruction can be figured out by counting the number of reconstructed K^0_S in the more stringent tagged sample in which at least a pair of $\pi^+\pi^-$ tracks are required. The obtained efficiencies for the secondary vertex reconstruction are also drawn in Fig. 5(c). From the figure, it can be seen that detection efficiency loss is mainly caused by tracking efficiencies, especially in the larger decay length regions.

5.3 Results and systematical estimations

The experimental resolution and detection efficiency functions have been determined in the control sample. The probability density function (p.d.f.) for lifetime measurements is constructed according to Eq. (7) and fits the data. The proper time ($c\tau$) distribution in the test sample is shown in Fig. 5(d). The fitting procedure is done by the RooFit package[9] in which a technique of numeric convolution integration is applied to normalize the p.d.f.. Finally we get $c\tau = (2.66 \pm 0.02)$ cm which is consistent with the input value of 2.68 cm; the error is statistical only.

The major systematic uncertainties in the K^0_S lifetime measurements come from the determination of the experimental resolution and the detection efficiency function, the PID (particle identification) and tracking efficiencies and the disagreement between data and Monte Carlo. The systematic uncertainties due to ${\rm d}E/{\rm d}x$ PID can be estimated by tracks from the interaction point. For the TOF PID the flight time should be decompressed in two steps: 1) the flight time of the K^0_S from the production vertex to the decay vertex and 2) the flight time of the daughter charged pion from the decay vertex to the TOF counter. After the flight time correction, the systematic uncertainties due to TOF PID could be estimated. The additional systematic uncertainties of the lifetime of the reference particle should be interpreted as the disagreement between the data and the Monte Carlo.

The systematic uncertainties in the experimental resolution can be estimated by modeling the resolution function from different samples, e.g. the sample of ρ^0 and K^{*0} decays. The systematic uncertainties in the detection efficiencies can be addressed by changing the efficiency curve from a 2nd-order polynomial to a 1st-order and/or 3rd-order polynomial. To evaluate the systematic uncertainties in the tracking procedure two track finding algorithms[10, 11] are investigated. The estimates are summarized in Table 1. The uncertainties in particle identification and the disagreement between the data and Monte Carlo are not included in this estimation.

Table 1. Systematic uncertainties in the lifetime measurement.

item	uncertainties/cm
experimental resolution	±0.01
detection efficiencies	±0.02
track finding algorithm	±0.03

6 Discussion

Currently the secondary vertex reconstruction algorithm has been implemented in C++ language and been applied to physics analysis. It uses the track parameters at the closest point to the origin. While the decay vertex is outside the beam pipe or outside the inner radius of the drift chamber, material effects, such as multiple scattering and energy loss for charged tracks, may be corrected improperly. The Kalman track fitting algorithm provides two sets of track parameters at the closest point to the origin and at the point of the first hit layer in the drift chamber. To investigate the effect of material corrections, $J/\psi \to \Lambda\bar{\Lambda}$ events are generated. The Λ baryons are reconstructed by using different initial track parameters. We find that the invariant mass of $\Lambda/\bar{\Lambda}$ is always the same around its nominal value; however, the reconstructed momentum has some offsets. Fig. 6 shows the relation of ΔP and R, where $\Delta P = P_{\rm rec} - P_{\rm gen}$ is the difference between the reconstructed momentum ($P_{\rm rec}$) and the generated momentum ($P_{\rm gen}$), $R = \sqrt{x^2+y^2}$ is the traversed distance of the Λ decay vertex in the x-y plane.

About 4 MeV differences are caused by applying different initial daughter track parameters. For $R < 3$ cm, corresponding to the inner radius of the beam pipe, the initial daughter track parameters at the closest point to the origin may give correct results. For $R > 6$ cm, corresponding to the inner radius of the drift chamber, the initial daughter track parameters at the first MDC hit layer may return a correct ΔP. But for 3 cm $< R <$ 6 cm, both sets of initial track parameters are not properly corrected. It seems that the current configuration of the Kalman track fitting is not perfect for the tracks of the decay daughters. A suggestion is naturally brought forward: the material effects should be corrected to the decay position in the Kalman track fitting procedure. So it is crucial to combine the vertex reconstruction and Kalman track fitting. The daughter tracks must be refitted if the decay vertex is found to be outside the beam pipe. Such work is in progress[12].

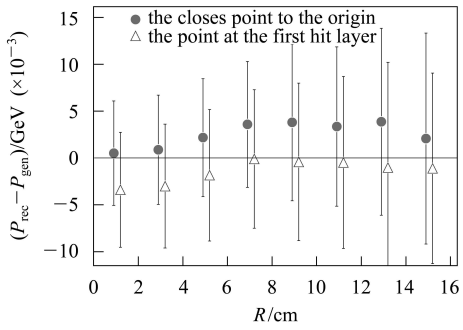

Fig. 6. ΔP versus R for Λ baryons using different initial track parameters. Full circles: the initial daughter track parameters at the closest point to the origin have been used, triangles: the initial daughter track parameters at the first hit layer in the drift chamber have been used.

References

1 BESIII Design Report, Interior Document in Institute of High Energy Physics, 2004
2 Harris F A (BES Collab.). arXiv: physics/0606059
3 LI W D, LIU H M et al. The Offline Software for the BESIII Experiment. Proceeding of CHEP06. Mumbai, 2006
4 DENG Z Y et al. HEP & NP, 2006, **30**(5): 371—377 (in Chinese)
5 Agostinelli S et al (Geant4 Collab.). Nucl. Instrum. Methods A, 2003, **506**: 250
6 XU Min. The Report on Vertex Reconstruction, July 2008, BESIII annual meeting
7 Paul Avery. Fitting Theory Writeups and References
8 Particle Data Group. 2008
9 Verkerke W, Kirkby D. RooFit Users Manual v2.07, Jan 2006
10 ZHANG Y et al. HEP & NP, 2007, **31**(6): 570—575 (in Chinese)
11 LIU Q G et al. Chinese Physics C, 2008, **32**(7): 565—571
12 WANG J K. The Report on MDC Kalman Track Fitting, July 2008, BESIII annual meeting